

Article

Fabrication of Hollow Silica Nanospheres with Ultra-High Acid Density for Efficient Heterogeneous Catalysis

Xiaoli Zhang ¹, Juan Wei ^{2,*} and Xiaoming Zhang ^{3,*} 

¹ Shaanxi Key Laboratory of Natural Products & Chemical Biology, College of Chemistry & Pharmacy, Northwest A&F University, 22 Xinong Road, Yangling 712100, China; xiaoliflyhighly@163.com

² School of Chemical and Environmental Engineering, Sichuan University of Science and Engineering, Zigong 643000, China

³ School of Chemistry and Chemical Engineering, Shanxi University, Wucheng Road 92, Taiyuan 030006, China

* Correspondence: jwei@suse.edu.cn (J.W.); xmzhang4400@sxu.edu.cn (X.Z.)

Received: 6 May 2019; Accepted: 21 May 2019; Published: 24 May 2019



Abstract: Hollow silica nanospheres with ultra-high acid density were fabricated successfully via sulfonation of phenyl-functionalized hollow silica nanospheres, which were synthesized through a single micelle (F127 (EO₁₀₆PO₇₀EO₁₀₆))-templated method, with phenyltrimethoxysilane and tetramethoxysilane (TMOS) as silane precursors under neutral conditions. The density of sulfonic acid reached as high as 1.97 mmol/g. The characterization results of ³¹P-NMR using triethylphosphine oxide as a probe molecule suggested that the acid strength of hybrid solid acids could be systematically tuned by tuning the content of sulfonic acid and higher acid density results in stronger acid strength. Attributed to the unique hollow structure and high-acid density, the sulfonic acid-functionalized hollow silica nanospheres exhibited good catalytic performance in the condensation reaction of benzaldehyde with ethylene glycol. Notably, this study found that the catalytic activity was significantly influenced by the acid density and the ultra-high acid loading was beneficial for the activity due to the enhanced acid strength. This novel solid-acid catalyst also showed good recyclability and could be reused for at least 11 runs.

Keywords: solid-acid catalysis; hollow silica nanospheres; high-acid density; condensation reaction of benzaldehyde

1. Introduction

Replacing hazardous and corrosive mineral liquid acids with solid acids is meaningful for the industrial production of fine chemicals with environmental and safety considerations [1–4]. Solid acids, including zeolites, sulfonated metal oxides, heteropolyacids, and ion-exchange resins, have been developed and applied in various acid-catalysed reactions, such as esterification, Beckmann rearrangement, olefin hydration, condensation reaction, alkylation of phenols, etc. [5–14]. Among these solid acid catalysts, sulfonic acid-functionalized mesoporous silica have attracted much research interest owing to their superior advantages, such as high surface area and pore volume, large pore size, and good thermal stability [15–20]. These features make them promising alternatives to commercial sulfonated polymer resins (like Amberlyst-15, Nafion-H) which suffer from the drawbacks of low surface area. In addition, it provides a new way to settle the limitations of micropores in zeolites for transformation of bulky molecules.

The sulfonic acid-functionalized mesoporous silica catalysts are typically synthesized by attaching sulphur or phenyl-containing organic silanes on the pore walls of mesoporous silica materials via post-grafting or co-condensation methods followed by oxidation with hydrogen peroxide or sulfonation

with $\text{H}_2\text{SO}_4/\text{ClSO}_3\text{H}$ [21–24]. However, the dosage of functionalized silanes in these processes must be carefully controlled to avoid the destruction of ordered mesostructures or the possibility of pore blocking. In most situations, only a limited functional silane amount is allowed to be used, which often leads to a low-acid density in the pore walls [25–27]. Nevertheless, the acid density influences the acid strength and catalytic activity significantly and is an important parameter for practical applications [28]. Therefore, synthesizing functionalized mesoporous heterogeneous solid-acid catalysts with high-acid density is of great importance and interest.

Different strategies have been employed to increase the acid density of sulfonic acid-functionalized mesoporous silicas [15,25,26,29]. For example, Wilson [25] reported the synthesis of SBA-15 with ultra-high sulfonic acid loading (2.2 mmol/g H^+) through a hydrothermal silane-promoted grafting method. Yang's group [15,29] also reported a confined polystyrene sulfonic acid resins catalyst with local acid loading as high as 2.0 mmol/g. Though these strategies are efficient, the design of solid acid with tunable acidity is still a goal being pursued in the development of excellent solid-acid catalysts. Furthermore, the most reported sulfonic acid-functionalized mesoporous silica catalysts have no a well-defined morphology, which is important for the accessibility of active sites and fast diffusion of the reactants and products.

Solid catalysts with hollow nanosphere morphology have attracted much attention recently, since their catalytic performances can be improved by their shortened diffusion lengths [30–35]. However, the acid loading is usually limited because the morphology and structure will be damaged with high organic group content [36]. Here, we report the construction of hollow silica nanospheres with ultra-high acid loading (1.97 mmol/g, denoted as $\text{SO}_3\text{H-Ph-HNS-x}$) via sulfonation of phenyl-functionalized hollow silica nanospheres (denoted as Ph-HNS-x), which were fabricated by a one-pot hydrothermal method with phenyltrimethoxysilane and tetramethoxysilane (TMOS) as precursors (x is the mass ratio of added phenyltrimethoxysilane with TMOS) and F127 ($\text{EO}_{106}\text{PO}_{70}\text{EO}_{106}$) as a single micelle template under neutral conditions. Systematic study of the relationship of the acid loading, acid strength, and catalytic performance was conducted.

2. Results and Discussion

2.1. Synthesis and Characterization of the Solid-Acid Catalyst $\text{SO}_3\text{H-Ph-HNS-x}$

The solid-acid catalyst $\text{SO}_3\text{H-Ph-HNS-x}$ was obtained by sulfonation of phenyl-functionalized hollow nanospheres with a commonly used chlorosulfonic acid. F127 was used as a soft template for the preparation of phenyl-functionalized hollow nanospheres under neutral conditions [37,38]. Because of the lower hydrolysis rate of phenyltrimethoxysilane, a pre-hydrolysis strategy was utilized in the synthesis process, and samples with different contents of phenyl groups were prepared.

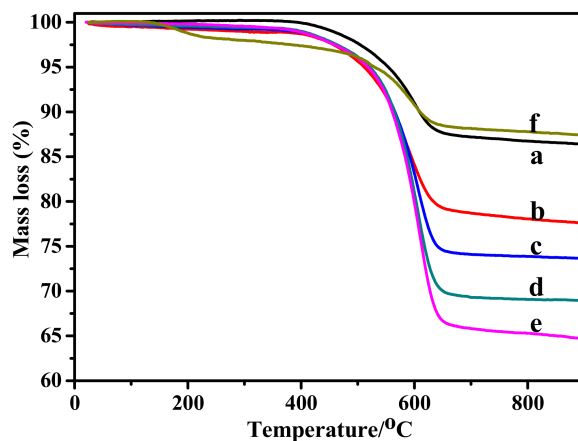


Figure 1. TGA curves of phenyl-functionalized hollow nanospheres before sulfonation: (a) Ph-HNS-1/6, (b) Ph-HNS-1/3, (c) Ph-HNS-1/2, (d) Ph-HNS-3/4, (e) Ph-HNS-1/1, and (f) Ph-HNS-G.

Firstly, the content of phenyl groups incorporated into the hollow silica nanospheres was determined by the weight loss of TGA (thermogravimetric analysis) curves in the range of 400–800 °C (Figure 1 and Table 1). As shown, the content of phenyl groups could be verified in the range of 13.5% to 34.1%, as the mass ratio of phenyltrimethoxysilane during the synthesis process increased from 1/6 to 1/1, indicating that the phenyl content could be adjusted by changing the initial dosage of organosilanes. Compared with phenyl-functionalized hollow nanospheres prepared by the traditional grafting method, Ph-HNS-1/1 showed a much higher content of phenyl groups (34.1 versus 11.0 wt%) and a little higher decomposition temperature of phenyl groups.

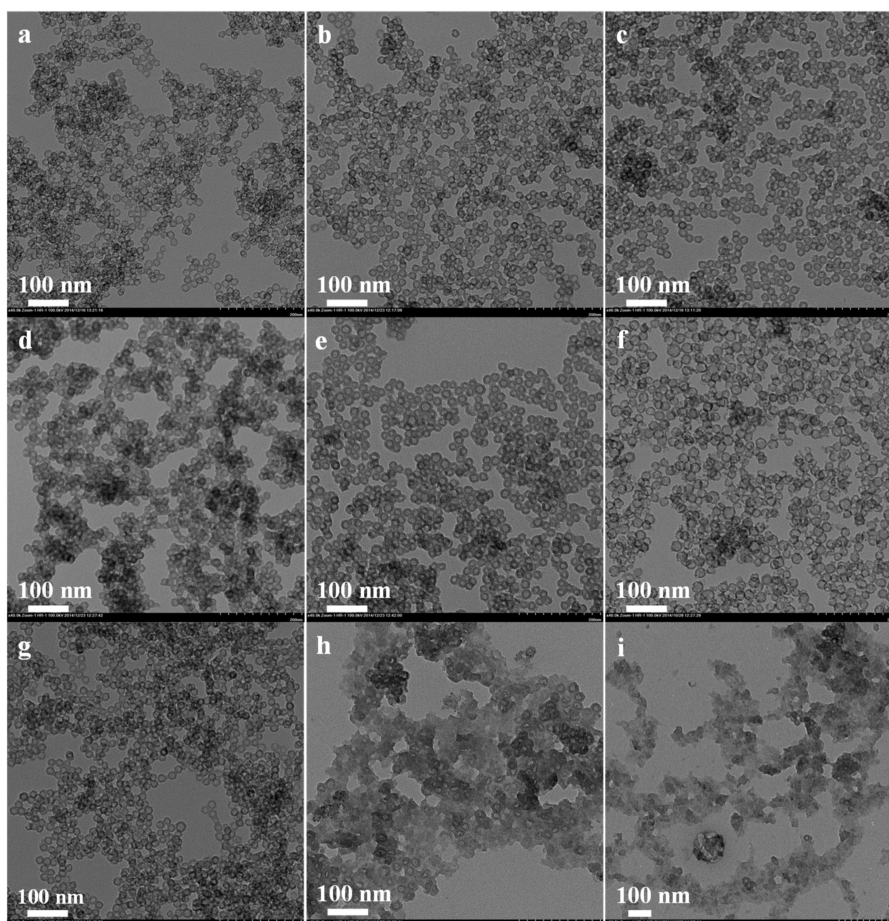


Figure 2. TEM images of (a) SO₃H-Ph-HNS-1/6, (b) SO₃H-Ph-HNS-1/3, (c) SO₃H-Ph-HNS-1/2, (d) SO₃H-Ph-HNS-3/4, (e) SO₃H-Ph-HNS-1/1, (f) SO₃H-Ph-HNS-G, (g) Ph-HNS-1/1, and (h) and (i) SO₃H-Ph-HNS-1/6 and SO₃H-Ph-HNS-1/1 without thermal treatment.

The TEM images of obtained SO₃H-Ph-HNS-*x* solid catalysts are shown in Figure 2. All the samples exhibited uniform hollow nanosphere structures as the mass ratio of phenyltrimethoxysilane increased from 1/6 to 1/1 (Figure 2a–e), which was similar to the sulfonated post-grafting sample (Figure 2f). The sizes of the hollow nanospheres were measured to be 18 ± 2 nm with a shell thickness of 3.5 ± 0.5 nm while leaving a large hollow cavity. Notably, the hollow nanosphere with high phenyltrimethoxysilane ratio of 1/1 possessed almost the same morphology and particle size, indicating that the synthesis method is applicable for incorporating abundant organic groups (Figure 2g). Notably, a thermal treatment (at 350 °C for 2 h) before sulfonation was needed to obtain such intact hollow nanospheres, and without thermal treatment, the sulfonated samples would break (Figure 2h,i), which might be ascribed to the relatively low condensation level of TMOS under neutral conditions.

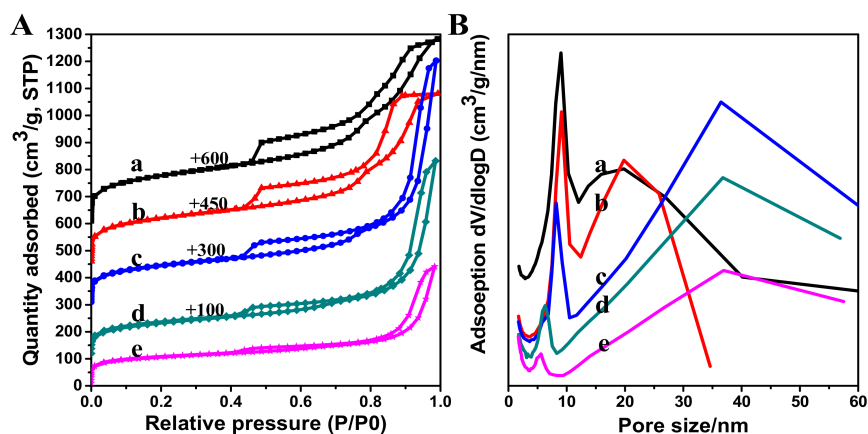


Figure 3. Nitrogen-sorption isotherms (A) and pore size distributions (B) of (a) SO₃H-Ph-HNS-1/6, (b) SO₃H-Ph-HNS-1/3, (c) SO₃H-Ph-HNS-1/2, (d) SO₃H-Ph-HNS-3/4, (e) SO₃H-Ph-HNS-1/1.

The nitrogen-sorption isotherms and pore size distribution curves of the hollow nanosphere catalyst SO₃H-Ph-HNS-*x* are presented in Figure 3, and their corresponding textural parameters are listed in Table 1. As shown, the adsorption-desorption isotherms of the samples displayed type IV isotherm patterns which is typical for mesoporous silicas. The adsorption isotherms of these samples exhibited two capillary condensation steps, indicating that two types of mesopores existed. This was also verified by the corresponding pore size distribution curves (Figure 3B). The first hysteresis loop appeared at relative pressure P/P_0 of 0.50–0.80, which might have originated from the interior space of the hollow nanospheres, while the second capillary condensation ($P/P_0 = 0.80–1.0$) might be from the void space among aggregated nanospheres. The interior cage sizes of the hollow nanospheres were determined to be about 9.2–5.5 nm, using a Barrett–Joyner–Halenda (BJH) calculation method, which were smaller than the TEM observations. This phenomenon can be easily explained, since the BJH calculation method is often for cylindrical pore size analysis and might underestimate the pore of cage type materials. Sulfonated hybrid hollow nanospheres possess high Brunauer–Emmett–Teller (BET) surface area and pore volume, which will be beneficial for the fast diffusion of the substrates and products. The BET surface area and pore size decreased from 629 to 366 m²/g and 9.2 to 5.5 nm, respectively, as the phenyltrimethoxysilane ratio increased from 1/6 to 1/1, probably due to the occupation of organic groups in the interior nanocages. Compared with SO₃H-Ph-HNS-G, most of the solid catalyst SO₃H-Ph-HNS-*x* exhibited higher surface area, revealing the superiority of the one-pot hydrothermal method to the traditional post-grafting method.

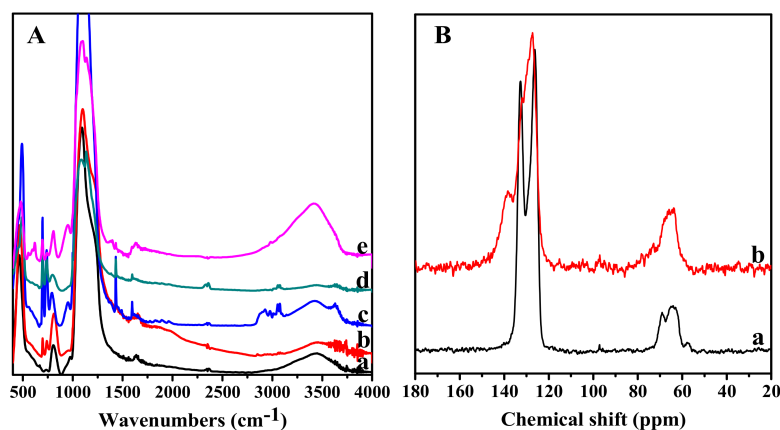


Figure 4. (A) FTIR spectra of (a) pure silica HNS, (b) Ph-HNS-G, (c) Ph-HNS-1/1, (d) Ph-HNS-1/1 after thermal treatment, and (e) SO₃H-Ph-HNS-1/1; (B) Solid ¹³C NMR spectra of (a) Ph-HNS-1/1 and (b) SO₃H-Ph-HNS-1/1.

Table 1. Textural parameters of SO₃H-Ph-HNS-x and weight loss of Ph-HNS-x.

Sample	BET Surface Area (m ² /g)	Pore Volume (cm ³ /g) ¹	Cage Size (nm) ²	Phenyl Content (wt%) ³
SO ₃ H-Ph-HNS-1/6	629	1.06	9.2	13.5
SO ₃ H-Ph-HNS-1/3	600	0.98	9.1	21.1
SO ₃ H-Ph-HNS-1/2	507	1.40	8.3	25.2
SO ₃ H-Ph-HNS-3/4	465	1.13	6.3	30.0
SO ₃ H-Ph-HNS-1/1	366	0.68	5.5	34.1
SO ₃ H-Ph-HNS-G	394	2.03	13.3	11.0

¹ Single-point pore volume calculated at relative pressure P/P₀ of 0.99. ² Barrett-Joyner-Halenda (BJH) method from the adsorption branch. ³ Mass loss between 400–800 °C.

To verify the successful introduction of –SO₃H groups, several representative samples were characterized by FTIR spectra. As exhibited in Figure 4A, two strong bands around 3680–3130 and 1350–1000 cm^{−1} were clearly observed for all of the samples, which can be ascribed to characteristic bands of ν (O–H) and ω (Si–O) for silica materials. Due to the decreased amount of Si–OH after post-grafting with the phenyl group, the strength of Ph-HNS-G around 3680–3130 cm^{−1} was weakened, suggesting the successful grafting of the phenyl group. Compared with pure silica HNS, the other samples exhibited weak bands around 3100–3000 cm^{−1}, 1540–1450 cm^{−1}, and 730–650 cm^{−1}, which are assigned to the C–H stretching vibration, the C=C vibration, and breathing vibration of phenyl-ring groups. Notably, the sulfonated sample also exhibited additional bands at 610 and 1380 cm^{−1} that were associated with sulfonic groups. This observation confirmed the successful sulfonation of the phenyl-functionalized samples, which was further demonstrated by solid ¹³C NMR spectra. As shown in Figure 4B, compared with Ph-HNS-1/1, SO₃H-Ph-HNS-1/1 clearly showed the signal assigning to the aromatic carbon that coordinated with –SO₃H groups at around 138 ppm, further confirming the successful anchoring of the sulfonic acid group on aromatic rings of the hollow nanospheres.

To quantitatively analyse the contents of the sulfonic acid in the hollow nanospheres, the sulphur content was obtained by elemental analysis, while the acid exchange capacity was obtained through an acid-based titration method. As listed in Table 2, as the content of the phenyl groups in the hollow nanosphere increased, higher sulphur content and acid exchange capacity could be obtained. Moreover, while the S elemental content increased from 0.90 to 1.78 mmol/g, the acid exchange capacity of SO₃H-Ph-HNS-x varied from 1.16 to 1.97 mmol/g. The amount of H⁺ and S were similar, suggesting that most of the acid sites were exposed during the titration process. The slight difference might be attributed to existing errors in the measuring methods. According to the amount of acid exchange capacity, the acid density on the hollow nanosphere was in the range of 0.86–2.93 nm^{−2}.

The acid strength of SO₃H-Ph-HNS-x and SO₃H-Ph-HNS-G were then characterized by a ³¹P MAS NMR technique using TEPO (triethylphosphine oxide) as a probe molecule. Such a unique method was found to be practical for acidity characterization, since the ³¹P chemical shift of TEPO chemisorbed on the sulfonic acid site was very sensitive to acid strength. Stronger acid usually leads to a larger chemical shift of TEPO. As shown in Figure 5, SO₃H-Ph-HNS-1/1 with the highest acid content had the strongest acid strength and SO₃H-Ph-HNS-1/6 showed the lowest acid strength due to its low acid content. Encouragingly, the chemical shift of SO₃H-Ph-HNS-1/1 was similar to that of Amberlyst-15 (88.3 versus 89.4 ppm). All the samples prepared by the one-pot co-condensation method have stronger acid strength than SO₃H-Ph-HNS-G, as verified by the larger chemical shift of the former samples. The chemical shift of most samples followed the same sequence of the acid content with the exception of SO₃H-Ph-HNS-1/3. This sample with moderate acid content had stronger acid strength than SO₃H-Ph-HNS-1/2 and SO₃H-Ph-HNS-3/4 with higher acid content, which might be related to the location of sulfonic acid groups within the SO₃H-Ph-HNS. For samples Ph-HNS-x (x = 1/6, 1/3) with low phenyl content, the phenyl groups were preferentially distributed in the inner surface under the single micelle synthesized system since that was the hydrophobic region of the micelle. The concentration of phenyl groups in the inner part generated high acid site density on the

inner surface, and the interaction between $-\text{SO}_3\text{H}$ groups was enhanced, which was helpful to enhance the acid strength. The high SO_3H concentration in the inner region of Ph-HNS-1/6 also resulted in stronger acid strength than $\text{SO}_3\text{H-Ph-HNS-G}$, though its acid content was lower. Further increasing the loading of phenyl groups, the SO_3H will also be distributed on the outer surfaces, which was demonstrated by the small peaks at the chemical shift of 80–90 ppm.

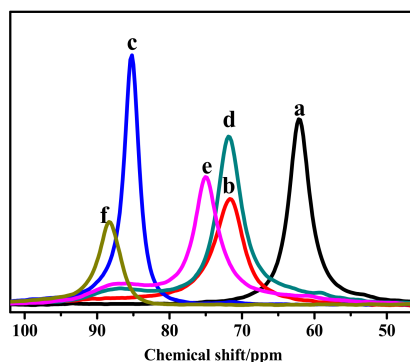
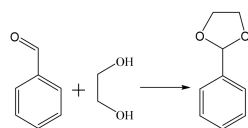


Figure 5. ^{31}P MAS NMR spectra of (a) $\text{SO}_3\text{H-Ph-HNS-G}$, (b) $\text{SO}_3\text{H-Ph-HNS-1/6}$, (c) $\text{SO}_3\text{H-Ph-HNS-1/3}$, (d) $\text{SO}_3\text{H-Ph-HNS-1/2}$, (e) $\text{SO}_3\text{H-Ph-HNS-3/4}$, and (f) $\text{SO}_3\text{H-Ph-HNS-1/1}$ (with TEPO as a probe molecule).

2.2. The Catalytic Performance of Sulfonated Hollow Nanospheres $\text{SO}_3\text{H-Ph-HNS-x}$

To investigate the catalytic performance of sulfonated hollow nanospheres, the condensation reaction of benzaldehyde with ethylene glycol, an important way to protect functional groups, was chosen as a model. The catalytic results are listed in Table 2. Under identical reaction conditions, all the sulfonated hollow nanospheres could efficiently catalyse the reaction with 88–90% conversion within 90 min. For $\text{SO}_3\text{H-Ph-HNS-x}$ catalysts, significant enhancement of the overall catalytic activity was observed as increasing the surface density of acid sites. For example, $\text{SO}_3\text{H-Ph-HNS-1/1}$ was about twice as active as $\text{SO}_3\text{H-Ph-HNS-1/6}$ (TOF: 563 vs 287 h^{-1} ; acid density: 2.93 vs 0.86 nm^{-2}). The higher activity might be attributed to the increased acid strength. Notably, the catalytic activity of $\text{SO}_3\text{H-Ph-HNS-1/1}$ was even similar to commercial Amberlyst-15 (89% conversion and TOF value = 596 h^{-1}) and much better than previously reported [13], further suggesting its good performance.

Table 2. The phenyl group content, sulfur content, and acid exchange capacity of sulfonated hollow nanospheres and their catalytic performance in the condensation reaction of benzaldehyde with ethylene glycol.



Catalyst	Ph Group Content (mmol/g) ¹	S Content (mmol/g) ²	Amount of Acid Sites (mmol/g) ³	Acid Site Density (nm^{-2}) ⁴	Conv. (%)	TOF (h^{-1}) ⁵
$\text{SO}_3\text{H-Ph-HNS-1/6}$	1.75	0.90	1.16	0.86	88	287
$\text{SO}_3\text{H-Ph-HNS-1/3}$	2.74	1.25	1.55	1.25	88	301
$\text{SO}_3\text{H-Ph-HNS-1/2}$	3.27	1.53	1.56	1.82	89	411
$\text{SO}_3\text{H-Ph-HNS-3/4}$	3.89	1.61	1.77	2.08	90	384
$\text{SO}_3\text{H-Ph-HNS-1/1}$	4.43	1.78	1.97	2.93	89	563
$\text{SO}_3\text{H-Ph-HNS-G}$	1.43	0.62	0.62	0.95	90	359
Amberlyst-15	-	-	4.7	-	89	596

Reaction conditions: solid catalyst, benzaldehyde (106.1 mg, 1 mmol), ethylene glycol (62.1 mg, 1mmol) and 3.0 mL of cyclohexane, S/C = 50, 90 °C, toluene as internal standard, for 90 min. ¹ Calculated with TG results. ² S element analysis. ³ Determined through ion exchange and titration. ⁴ Number of acid sites divided by surface area. ⁵ Turn over frequency, calculated with the initial conversion of benzaldehyde.

The variation in activity for $\text{SO}_3\text{H-Ph-HNS-x}$ cannot, however, be mainly attributed to the acid strength. The distribution of $-\text{SO}_3\text{H}$ groups within the hollow nanospheres is another influential factor. For Ph-HNS-x ($x = 1/6, 1/3$) with low acid content samples, most of the $-\text{SO}_3\text{H}$ groups might be distributed in the interior surface, and in-pore diffusion limitations will be increased. As shown in Figure 6, compared with $\text{SO}_3\text{H-Ph-HNS-G}$, these samples showed lower catalytic activity though they possess higher acid strength (TOF 287, 301 versus 359 h^{-1}), which might be due to the effect of in-pore diffusion limitations. Further increasing the acid content, $-\text{SO}_3\text{H}$ groups will distribute on the outer surface, and the interaction between $-\text{SO}_3\text{H}$ groups in these samples becomes more significant. However, $\text{SO}_3\text{H-Ph-HNS-3/4}$ showed a little lower activity than $\text{SO}_3\text{H-Ph-HNS-1/2}$ (TOF 384 versus 411 h^{-1}), which might be related with their different support surface area (507 versus $465 \text{ m}^2/\text{g}$).

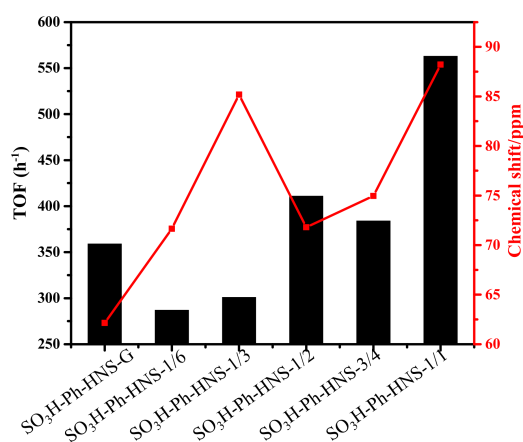


Figure 6. The acid strength (chemical shift) and catalytic activity (TOF values) of different samples.

The catalytic stability of sulfonated hollow nanospheres was tested using $\text{SO}_3\text{H-Ph-HNS-1/1}$ as a model catalyst. The solid catalyst was isolated by centrifugation, washed thoroughly with cyclohexane. After being dried in a vacuum, the solid catalyst was used in the next cycle. As shown in Figure 7A, above 90% of conversion could be well maintained even after running 11 cycles, suggesting a good reusability. Moreover, to better evaluate the recyclability, TOF values for each reaction cycle were also calculated. As exhibited, the TOF of the solid catalyst could be maintained within 11 cycles, although a slight decrease was observed (563 to 440 h^{-1}). After recycling, the hollow nanospheres were also characterized by TEM. As shown in Figure 7B, the hollow structure was still maintained, indicating a good stability of the solid catalyst.

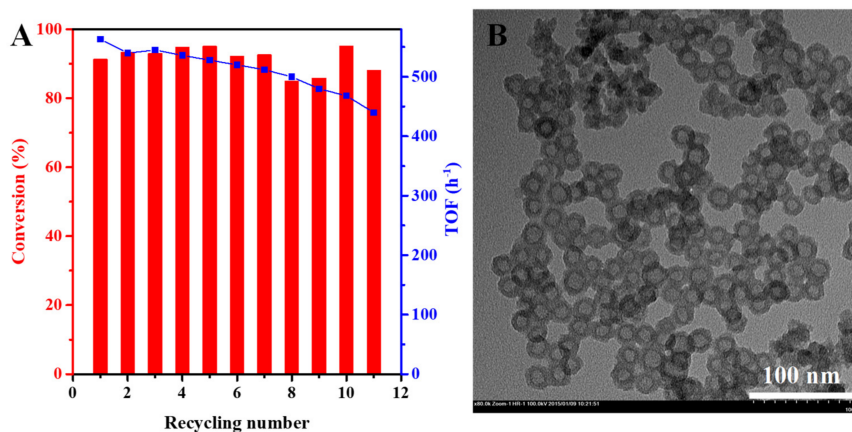


Figure 7. (A) Recycling stability of $\text{SO}_3\text{H-Ph-HNS-1/1}$ in the condensation reaction of benzaldehyde with ethylene glycol; (B) TEM image of $\text{SO}_3\text{H-Ph-HNS-1/1}$ after recycling test.

3. Materials and Methods

3.1. Chemicals and Materials

All of the commercial chemicals were used directly without any further purification. Phenyltrimethoxysilane was purchased from Alfa Aesar. Pluronic F127 ($M_w = 12,600$, $EO_{106}PO_{70}EO_{106}$) was obtained from Sigma–Aldrich. Other used reagents were from Shanghai Chemical Reagent Company of the Chinese Medicine Group.

3.2. Synthesis of Phenyl-Functionalized Hollow Silica Nanospheres (Ph-HNS- x)

For a typical procedure, 24 mL of deionized water was added to a conical flask containing 0.40 g of F127 and 1.40 g of K_2SO_4 . After dissolving at 13.5 °C under vigorous stirring, a mixture of TMB (0.40 g) and phenyltrimethoxysilane (0.20 g, 0.40 g, 0.60 g, 0.90 g or 1.20 g) were quickly added under stirring. After pre-hydrolysis for about 3 h, TMOs (1.20 g) were injected and a mixture with molar composition of TMOs/F127/phenyltrimethoxysilane/TMB/ K_2SO_4 /H₂O = 1:0.0040: x :0.42:1.02:169 ($x = 0.13, 0.26, 0.39, 0.585$ or 0.78) was obtained. After further stirring at 13.5 °C for 24 h, the resultant mixture was transferred to an oven and kept static at 100 °C for another 24 h. The solid product was isolated by filtration and washed with water and ethanol. Then, the F127 surfactant was removed by refluxing the obtained solid material (1.0 g) in a HCl–ethanol solution (1.5 g 36.5 wt% HCl in 200 mL of EtOH) for 24 h. After filtration and thoroughly washing with ethanol, the samples were dried. The final products were denoted as Ph-HNS- x ($x = 1/6, 1/3, 1/2, 3/4$ or $1/1$), where x is the mass ratio of added phenyltrimethoxysilane with TMOS.

For comparison, the phenyl-modified hollow nanosphere was also synthesized through a post-grafting method. The hollow nanospheres without phenyl group were synthesized as described above, except no phenyltrimethoxysilane was added. The surfactant was removed by calcination. Then, 0.50 g of pure silica nanosphere was dispersed into 30 mL of toluene, followed by the addition of Et₃N (1.0 mL) and phenyltrimethoxysilane (1.0 mL). The mixture was refluxed at 110 °C for 24 h under an Ar atmosphere. The solid product was centrifugated and washed with toluene and ethanol. The sample was denoted as Ph-HNS-G.

3.3. Synthesis of Sulfonated Ph-HNS Catalyst (SO_3H -Ph-HNS- x)

The synthesized phenyl-modified hollow nanospheres were firstly treated under 350 °C in air for 2 h. After thermal-treatment, 1.0 g of the sample was weighed in a round flask. After cooling to 0 °C, 40 mL of CH_2Cl_2 and 10 mL of chlorosulfonic acid were added. Then, the mixture was stirred for 12 h. After centrifugation, the solid catalyst was thoroughly washed with a large amount of water until the filtrate was neutral. The powder products were dried in vacuum at 60 °C overnight. The yielded solid catalyst was denoted as SO_3H -Ph-HNS- x .

3.4. Characterization

Nitrogen physical adsorption measurement was performed on the micromeritics ASAP2020 volumetric adsorption analyser. The samples were degassed at 393 K for 5 h before the measurements. The BET surface area, total pore volume, and pore diameter were determined from the data at P/P_0 of 0.05 to 0.25, the adsorbed amount at P/P_0 value of 0.99, and the adsorption branch with a BJH method, respectively. Transmission electron microscopy (TEM) was conducted using a FEI Tecnai G2 Spirit (Hongkong, China) with an acceleration voltage of 120 kV. The FTIR spectra were collected with a Nicolet Nexus 470 IR spectrometer (Wisconsin, United States). Thermogravimetric analysis (TGA) was carried out using a NETZSCH STA-449F3 thermogravimetric analyser (Selb, Germany), with 5 °C/min of heating rate under air atmosphere. The MAS ¹³C NMR spectra were obtained on a Bruker DRX-400 (Rheinstetten, Germany) with analysed parameters as 8 kHz spin rate, 3 s pulse delay, 4 min contact time, and 1000 scans. The ³¹P NMR spectra were performed at a frequency of 242.9 MHz using a 4 mm MAS probe on a Bruker Avance III 600 spectrometer (Rheinstetten, Germany), while

high-power proton decoupling with a spinning rate of 12 kHz was utilized. The chemical shift spectra were referenced to an external standard (85 wt% phosphoric acid).

An acid-based titration method was utilized to determine the acid exchange capacity. Typically, 0.05 g of solid catalyst was firstly degassed under 120 °C, and then dispersed into 25 mL of 2 M NaCl aqueous solution. After stirring at room temperature for 24 h, equilibrium was reached. Subsequently, the solution was titrated with standard NaOH solution.

3.5. The Condensation Reaction of Benzaldehyde with Ethylene Glycol

The reaction was performed in a 10-mL Schlenk tube with a reflux condenser. Typically, a desired amount of solid catalyst SO₃H-Ph-HNS-x (S/C = 50) was added into the tube reactor containing a mixture of benzaldehyde (1 mmol, 106.1 mg) and ethylene glycol (1.0 mmol, 62.1 mg) in 3 mL of cyclohexane. The reaction was performed at 90 °C under stirring. After reaction, the solution was analysed by GC equipped with a FID detector and a HP-5 capillary column (30 m × 0.32 mm ID, 0.5 μm film, temperature program 100 °C for 15 min). For recycling tests, the solid catalyst was filtered from the reaction solution and thoroughly washed with cyclohexane. After being dried under vacuum, the powder was used in the next cycle.

4. Conclusions

In conclusion, we have proposed an efficient sulfonic hybrid hollow nanosphere catalyst with tunable acid content for catalysis applications. The sulfonic acid site loading reached as high as 1.97 mmol/g while maintaining a hollow nanosphere structure. The effects of acid site density on the overall acidity and catalytic performance were investigated. The study showed that higher acid density could increase the acid strength, leading to an increase in the catalytic activity. Our results are helpful for designing novel functional hybrid silica nanoreactors for catalysis applications.

Author Contributions: Conceptualization, X.Z. (Xiaoming Zhang); methodology, J.W.; formal analysis, X.Z. (Xiaoli Zhang); investigation, X.Z. (Xiaoli Zhang); resources, J.W.; data curation, X.Z. (Xiaoming Zhang); writing—original draft preparation, J.W.; writing—review and editing, X.Z. (Xiaoming Zhang); visualization, J.W.; funding acquisition, J.W.

Funding: This work was supported by the National Natural Science Foundation of China (No. 21802100), Foundation of Sichuan University of Science and Engineering (No. 2017RCL47), the Zigong Science and Technology and Intellectual Property Bureau (No. 2016XC14).

Conflicts of Interest: The authors declare no conflict of interest.

References

1. Busca, G. Acid catalysts in industrial hydrocarbon chemistry. *Chem. Rev.* **2007**, *107*, 5366–5410. [[CrossRef](#)] [[PubMed](#)]
2. Corma, A.; Garcia, H. Lewis acids: from conventional homogeneous to green homogeneous and heterogeneous catalysis. *Chem. Rev.* **2003**, *103*, 4307–4365. [[CrossRef](#)] [[PubMed](#)]
3. Clark, J. Solid acids for green chemistry. *Acc. Chem. Res.* **2002**, *35*, 791–797. [[CrossRef](#)]
4. Wang, S.; Yang, G. Recent advances in polyoxometalate-catalyzed reactions. *Chem. Rev.* **2015**, *115*, 4893–4962. [[CrossRef](#)]
5. Dusselier, M.; Wouwe, P.; Dewaele, A.; Jacobs, P.; Sels, B. Shape-selective zeolite catalysis for bioplastics production. *Science* **2015**, *349*, 78–80. [[CrossRef](#)]
6. Dai, C.; Zhang, A.; Li, J.; Hou, K.; Liu, M.; Song, C.; Guo, X. Synthesis of yolk-shell HPW@hollow silicalite-1 for esterification reaction. *Chem. Commun.* **2014**, *50*, 4846–4848. [[CrossRef](#)]
7. Dou, J.; Zeng, H. Targeted synthesis of silicomolybdic acid (Keggin acid) inside mesoporous silica hollow spheres for Friedel–Crafts alkylation. *J. Am. Chem. Soc.* **2012**, *134*, 16235–16246. [[CrossRef](#)]
8. Joo, J.; Vu, A.; Zhang, Q.; Dahl, M.; Gu, M.; Zaera, F.; Yin, Y. A sulfated ZrO₂ hollow nanostructure as an acid catalyst in the dehydration of fructose to 5-hydroxymethylfurfural. *ChemSusChem* **2013**, *6*, 2001–2008. [[CrossRef](#)]

9. Liu, F.; Kong, W.; Qi, C.; Zhu, L.; Xiao, F. Design and synthesis of mesoporous polymer-based solid acid catalysts with excellent hydrophobicity and extraordinary catalytic activity. *ACS Catal.* **2012**, *2*, 565–572. [[CrossRef](#)]
10. Liu, F.; Meng, X.; Zhang, Y.; Ren, L.; Nawaz, F.; Xiao, F. Efficient and stable solid acid catalysts synthesized from sulfonation of swelling mesoporous polydivinylbenzenes. *J. Catal.* **2010**, *271*, 52–58. [[CrossRef](#)]
11. Zhang, F.; Wu, X.; Liang, C.; Li, X.; Wang, Z.; Li, H. Highly active, water-compatible and easily separable magnetic mesoporous Lewis acid catalyst for the Mukaiyama–Aldol reaction in water. *Green Chem.* **2014**, *16*, 3768–3777. [[CrossRef](#)]
12. Zhang, F.; Liang, C.; Wu, X.; Li, H. A nanospherical ordered mesoporous Lewis acid polymer for the direct glycosylation of unprotected and unactivated sugars in water. *Angew. Chem. Int. Ed.* **2014**, *53*, 8498–8502. [[CrossRef](#)] [[PubMed](#)]
13. Xing, R.; Liu, N.; Liu, Y.; Wu, H.; Jiang, Y.; Chen, L.; He, M.; Wu, P. Novel solid acid catalysts: Sulfonic acid group-functionalized mesostructured polymers. *Adv. Funct. Mater.* **2007**, *17*, 2455–2461. [[CrossRef](#)]
14. Liu, Y.; Liu, S.; He, D.; Li, N.; Ji, Y.; Zheng, Z.; Luo, F.; Liu, S.; Shi, Z.; Hu, C. Crystal facets make a profound difference in polyoxometalate-containing metal–organic frameworks as catalysts for biodiesel production. *J. Am. Chem. Soc.* **2015**, *137*, 12697–12703. [[CrossRef](#)]
15. Zhang, X.; Zhao, Y.; Xu, S.; Yang, Y.; Liu, J.; Wei, Y.; Yang, Q. Polystyrene sulphonic acid resins with enhanced acid strength via macromolecular self-assembly within confined nanospace. *Nat. Commun.* **2014**, *5*, 3170. [[CrossRef](#)]
16. Okada, T.; Miyamoto, K.; Sakai, T.; Mishima, S. Encapsulation of a polyoxometalate into an organosilica microcapsule for highly active solid acid catalysis. *ACS Catal.* **2014**, *4*, 73–78. [[CrossRef](#)]
17. Inumaru, K.; Ishihara, T.; Kamiya, Y.; Okuhara, T.; Yamanka, S. Water-tolerant, highly active solid acid catalysts composed of the Keggin-type polyoxometalate H₃PW₁₂O₄₀ immobilized in hydrophobic nanospaces of organomodified mesoporous silica. *Angew. Chem. Int. Ed.* **2007**, *46*, 7625–7628. [[CrossRef](#)]
18. Russo, P.; Antunes, M.; Neves, P.; Wiper, P.; Fazio, E.; Neri, F.; Barreca, F.; Mafra, L.; Pillinger, M.; Pinna, V. Mesoporous carbon–silica solid acid catalysts for producing useful bio-products within the sugar-platform of biorefineries. *Green Chem.* **2014**, *16*, 4292–4305. [[CrossRef](#)]
19. Wang, P.; Zhao, Y.; Liu, J. Versatile design and synthesis of mesoporous sulfonic acid catalysts. *Sci. Bull.* **2018**, *63*, 252–266. [[CrossRef](#)]
20. Alamillo, R.; Crisci, A.; Gallo, J.; Scott, S.; Dumesic, J. A tailored microenvironment for catalytic biomass conversion in inorganic–organic nanoreactors. *Angew. Chem. Int. Ed.* **2013**, *52*, 10349–10351. [[CrossRef](#)] [[PubMed](#)]
21. Wei, J.; Zou, L.; Li, J. Fabrication of mesoporous solid acid catalysts with tunable surface wettability for efficient catalysis. *New J. Chem.* **2016**, *40*, 4775–4780. [[CrossRef](#)]
22. Tucker, M.; Crisci, A.; Wigington, B.; Phadke, N.; Alamilo, R.; Zhang, J.; Scott, S.; Dumesic, J. Acid-functionalized SBA-15-type periodic mesoporous organosilicas and their use in the continuous production of 5-hydroxymethylfurfural. *ACS Catal.* **2012**, *2*, 1865–1876. [[CrossRef](#)]
23. An, S.; Sun, Y.; Song, D.; Zhang, Q.; Guo, Y.; Shang, Q. Arenesulfonic acid-functionalized alkyl-bridged organosilica hollow nanospheres for selective esterification of glycerol with lauric acid to glycerol mono- and dilaurate. *J. Catal.* **2016**, *342*, 40–54. [[CrossRef](#)]
24. Yang, Y.; Liu, X.; Li, X.; Zhao, J.; Bai, S.; Liu, J.; Yang, Q. A yolk–shell nanoreactor with a basic core and an acidic shell for cascade reactions. *Angew. Chem. Int. Ed.* **2012**, *51*, 9164–9168. [[CrossRef](#)]
25. Manayil, J.; Inocencio, C.; Lee, A.; Wilson, K. Mesoporous sulfonic acid silicas for pyrolysis bio-oil upgrading via acetic acid esterification. *Green Chem.* **2016**, *18*, 1387–1394. [[CrossRef](#)]
26. Wang, W.; Zhuang, X.; Zhao, Q.; Wan, Y. Self-assembly synthesis of a high-content sulfonic acid group functionalized ordered mesoporous polymer-based solid as a stable and highly active acid catalyst. *J. Mater. Chem.* **2012**, *22*, 15874–15886. [[CrossRef](#)]
27. Zhang, X.; Zhao, Y.; Yang, Q. PS-SO₃H@phenylenesilica with yolk–double-shell nanostructures as efficient and stable solid acid catalysts. *J. Catal.* **2014**, *320*, 180–188. [[CrossRef](#)]
28. Dacquin, J.; Cross, H.; Brown, D.; Duren, T.; Williams, J.; Lee, A.; Wilson, K. Interdependent lateral interactions, hydrophobicity and acid strength and their influence on the catalytic activity of nanoporous sulfonic acid silicas. *Green Chem.* **2010**, *12*, 1383–1391. [[CrossRef](#)]

29. Zhang, X.; Zhang, L.; Yang, Q. Designed synthesis of sulfonated polystyrene/mesoporous silica hollow nanospheres as efficient solid acid catalysts. *J. Mater. Chem. A* **2014**, *2*, 7546–7554. [[CrossRef](#)]
30. Li, Y.; Shi, J. Hollow-structured mesoporous materials: Chemical synthesis, functionalization and applications. *Adv. Mater.* **2014**, *26*, 3176–3205. [[CrossRef](#)]
31. Lee, J.; Kim, S.; Lee, I. Functionalization of hollow nanoparticles for nanoreactor applications. *Nano Today* **2014**, *9*, 631–667. [[CrossRef](#)]
32. Fang, X.; Liu, Z.; Hsieh, M.; Chen, M.; Liu, P.; Chen, C.; Zheng, N. Hollow mesoporous aluminosilica spheres with perpendicular pore channels as catalytic nanoreactors. *ACS Nano* **2012**, *6*, 4434–4444. [[CrossRef](#)]
33. Pérez-Lorenzo, M.; Vaz, B.; Salgueiriño, V.; Correa-Duarte, M. Hollow-shelled nanoreactors endowed with high catalytic activity. *Chem. Eur. J.* **2013**, *19*, 12196–12211. [[CrossRef](#)]
34. Sanlés-Sobrido, M.; Pérez-Lorenzo, M.; Rodríguez-González, B.; Salgueiriño, V.; Correa-Duarte, M. Highly active nanoreactors: nanomaterial encapsulation based on confined catalysis. *Angew. Chem. Int. Ed.* **2012**, *51*, 3877–3882. [[CrossRef](#)]
35. Zhang, X.; Jing, L.; Wei, L.; Zhang, F.; Yang, H. Semipermeable organic–inorganic hybrid microreactors for highly efficient and size-selective asymmetric catalysis. *ACS Catal.* **2017**, *7*, 6711–6718. [[CrossRef](#)]
36. Lu, B.; An, S.; Song, D.; Su, F.; Yang, X.; Guo, Y. Design of organosulfonic acid functionalized organosilica hollow nanospheres for efficient conversion of furfural alcohol to ethyl levulinate. *Green Chem.* **2015**, *17*, 1767–1778. [[CrossRef](#)]
37. Liu, J.; Yang, Q.; Zhang, L.; Yang, H.; Gao, J.; Li, C. Organic–inorganic hybrid hollow nanospheres with microwindows on the shell. *Chem. Mater.* **2008**, *20*, 4268–4275. [[CrossRef](#)]
38. Liu, J.; Fan, F.; Feng, Z.; Zhang, L.; Bai, S.; Yang, Q.; Li, C. From hollow nanosphere to hollow microsphere: Mild buffer provides easy access to tunable silica structure. *J. Phys. Chem. C* **2008**, *112*, 16445–16451. [[CrossRef](#)]



© 2019 by the authors. Licensee MDPI, Basel, Switzerland. This article is an open access article distributed under the terms and conditions of the Creative Commons Attribution (CC BY) license (<http://creativecommons.org/licenses/by/4.0/>).